Journal Pre-proofs

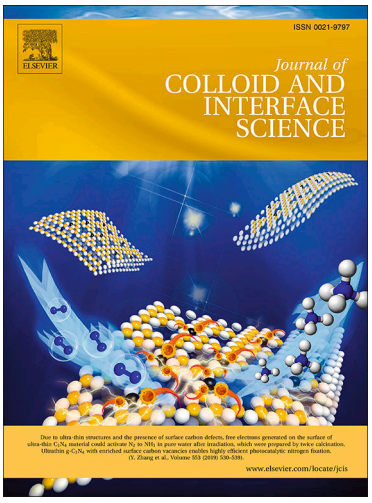

Regular Article

$Bi_2O_3/BiVO_4$@Graphene Oxide van der Waals Heterostructures with Enhanced Photocatalytic Activity toward Oxygen Generation

Yaxin Bi, Yanling Yang, Xiao-Lei Shi, Lei Feng, Xiaojiang Hou, Xiaohui Ye, Li Zhang, Guoquan Suo, Jingeng Chen, Zhi-Gang Chen

PII: S0021-9797(21)00225-3
DOI: https://doi.org/10.1016/j.jcis.2021.02.079
Reference: YJCIS 27623

To appear in: *Journal of Colloid and Interface Science*

Received Date: 5 December 2020
Revised Date: 25 January 2021
Accepted Date: 17 February 2021

Please cite this article as: Y. Bi, Y. Yang, X-L. Shi, L. Feng, X. Hou, X. Ye, L. Zhang, G. Suo, J. Chen, Z-G. Chen, $Bi_2O_3/BiVO_4$@Graphene Oxide van der Waals Heterostructures with Enhanced Photocatalytic Activity toward Oxygen Generation, *Journal of Colloid and Interface Science* (2021), doi: https://doi.org/10.1016/j.jcis.2021.02.079

$Bi_2O_3/BiVO_4$@Graphene Oxide van der Waals Heterostructures with Enhanced Photocatalytic Activity toward Oxygen Generation

Yaxin Bi[1,a], Yanling Yang[1,a,], Xiao-Lei Shi[2,a], Lei Feng[1], Xiaojiang Hou[1], Xiaohui Ye[1], Li Zhang[1], Guoquan Suo[1], Jingeng Chen[1], Zhi-Gang Chen[2,3,*]*

[1]School of Materials Science and Engineering, Shaanxi Key Laboratory of Green Preparation and Functionalization for Inorganic Materials, Shaanxi University of Science and Technology, Xi'an 710021, China

[2]Centre for Future Materials, University of Southern Queensland, Springfield, QLD 4300, Australia.

[3]Materials Engineering, the University of Queensland, Brisbane, QLD 4072, Australia.

[a] The first three authors contributed equally to this work

Corresponding Authors

* Yanling Yang: yangyanling@sust.edu.cn.

* Zhi-Gang Chen: zhigang.chen@usq.edu.au; zhigang.chen@uq.edu.au.

ABSTRACT

The van der Waals (vdW) integration enables to create heterostructures with intimate contact and bring new opportunities. However, it is not confined to layered materials but can also be generally extended to 3D materials. Multidimensional $Bi_2O_3/BiVO_4$@graphene oxide (GO) van der Waals heterostructures are synthesized by one-pot wet chemistry method. $Bi_2O_3/BiVO_4$ composite nanoparticles are self-assembled with GO framework by vdW interaction to form vdW heterostructures, in which GO framework allows short electron transport distance and rapid charge transfer and provides massive reactive sites. Such self-assembled heterostructures show a superior high photoactivity towards oxygen evolution with an enhanced oxygen generation rate of 1828 μmol h^{-1} g^{-1}, nearly 3 times than that of pure $BiVO_4$, attributed to the accelerated charge separation and transfer processes of $Bi_2O_3/BiVO_4$@GO vdW heterostructures. This study indicates that our strategy provides a new avenue towards fabricating multi-dimensional vdW heterostructures and inspiring more innovative insights in oxygen evolution field.

Keywords: $BiVO_4$, Graphene oxide, Van der Waals, Heterostructures, Oxygen evolution.

1. Introduction

Two-dimensional (2D) materials, including MoS_2 [1], graphite [2], WS_2 [3], $MoSe_2$ [4], have attracted worldwide attentions in the application in energy storage and conversion. Particularly, 2D graphene oxide (GO) has high specific surface, high strength, high stability, and high carrier mobility and shows great potentials in photocatalytic, thermal, and electrical fields [5]. Meanwhile, oxygen-rich functional groups of GO provide abundant reactive sites, which can enhance the interaction between their photocatalytic hybrid materials to facilitate electron transfer to enhance photocatalytic efficiency [6].

Currently, several universal strategies are used to assemble different 2D building blocks to form heterostructures by using physical or chemical interactions [7, 8]. Strong covalent bonds provide in-plane stability, whereas relatively weak, van-der-Waals-like forces are sufficient to keep the stack together. Therefore, these different 2D crystals can be stacked each another by using weak van der Waals (vdW) forces [9]. In fact, a few layered materials, such as Bi_2Te_3/FeTe [10], MoS_2/Au [11] and InSe/graphene heterostructures [12, 13] have been reported to link together by vdW forces for designing heterostructures. Atomic interfaces between layered materials accelerate the vdW interaction. Therefore, the vdW integration enables to create a great deal of heterostructures with intimate contact and bring new opportunities. Multilayer graphene vdW heterostructures were constructed using hexagonal boron nitride (h-BN) as a substrate [14, 15]. Similarly, graphene/MoS_2 [16] and BN/graphene/BN [17] were synthesized to improve charge mobility of graphene with the construction of 2D/2D

vdW integration. Such vdW integration can promote the separation of interfacial carriers and enable access to fast charge speed.

Actually, vdW interactions are not confined to interactions in layered materials and can also be generally extended to 3D materials [18]. Various multi-dimensional (2D/3D) heterostructures with multi-functionalities can be elaborately designed by using the different rational hybridization methods of different dimensional materials [19-21]. Their properties have been significantly enhanced by compensating individual weakness. Recently, a 2D/3D vdW heterostructure consisting of 2D triazine-based framework and 3D triazine-based graphdiyene has been reported for hydrogen evolution reaction [22]. A 3D/2D/2D structured $BiVO_4/FeVO_4$@rGO has been reported to have an enhanced transport and separation efficiency of photogenerated carriers [23]. Likewise, 2D/3D/2D rGO/Fe_2O_3/g-C_3N_4 nanocomposites were designed to inhibit the recombination rate of photoexcited charge carriers [24]. These fabricated multi-dimensional architectures, assembled with micrometer- and nanometer-scaled building blocks, exhibit unique photocatalytic activity compared to the individual structures [25, 26]. Therefore, such an approach provides various material choices and selectable properties and can be applicable for developing 3D systems.

In this work, we report a facile self-assembly of a multi-dimensional (2D/3D) $Bi_2O_3/BiVO_4$@GO vdW heterostructures via one-pot "wet" chemistry approach. The synthesized $Bi_2O_3/BiVO_4$ particle with a small diameter shows short electron transport distance. By stacking GO framework on $Bi_2O_3/BiVO_4$, 2D/3D heterostructures is formed and inherits the excellent properties of GO framework, including high specific surface

area and high carrier mobility. Such 2D/3D vdW heterostructures process massive reactive sites and accelerated electron transfer, thus have significantly enhanced photocatalytic activity toward oxygen generation.

2. Experiments

2.1 Synthesis of 2D/3D Bi_2O_3/$BiVO_4$@GO vdW heterostructures

All chemicals were obtained and used from commercial sources as analytical pure reagents without further purification. The 2D/3D Bi_2O_3/$BiVO_4$@GO vdW heterostructures were self-assembled by one-pot "wet" chemistry approach. 0.4 mmol $Bi(NO_3)_3 \cdot 5H_2O$ (Sinopharm Chemical Reagent Co., Ltd., 99 %) was firstly dissolved in 16 mL of glycerol after stirring for 1 hour (h). Then, 0.4 mmol $NaVO_3 \cdot 2H_2O$ (Sinopharm Chemical Reagent Co., Ltd., 99 %) was dissolved in another 16 mL of deionized water. It can be clearly seen that it gradually transformed into transparent and homogeneous after stirring for 0.5 h. The above solutions were mixed under continuous stirring, forming an orange suspension. The mixture with GO solution was then transferred into a Teflon-lined stainless steel autoclave and then heated to 180 ℃. Then, the as-synthesized nanoparticles were self-assembled by a facile solvothermal method to establish a vdW heterojunction of Bi_2O_3/$BiVO_4$@GO nanocomposites. For comparison, pure $BiVO_4$ was synthesized under the same conditions by hydrothermal method without the addition of GO solution. The experiment result shows that Bi_2O_3/$BiVO_4$@GO can be obtained after adding graphene oxide, indicating the GO is favorable for the formation of Bi_2O_3. The preparation approach can promote to fabricate mixed-dimensional vdW heterostructures in "wet" chemistry field.

2.2 Sample Characterization

The samples were detected by X-ray diffraction (XRD, D/Max-2200PC) and field-emission scanning electron microscope (SEM, Hitachi S4600). The transmission electron microscopy (TEM, JEM-2100F) was taken at current density of 10 uA with an accelerating voltage of 200 kV. Raman spectra were measured on Renishaw-invia Raman spectroscope. Ultraviolet-visible diffuse reflectance spectra (UV-Vis DRS) were characterized on a Cary 5000 spectrophotometer equipped with an integrating sphere, with $BaSO_4$ as a reflectance standard.

2.3 Photocatalytic Oxygen Evolution

Photocatalytic O_2 production is carried out under a 500 W Xe lamp. In the suspension, 50 mg catalysts were dispersed in 50 mL aqueous solution and $Fe(NO_3)_3$ was employed as the sacrifice agent. During the O_2 evolution, the solution was stirred and treated with nitrogen gas several times to remove the dissolved gases in the liquid. The experiment was conducted at room temperature by circulating cold water. After being irradiated for a period of time, the production of O_2 was analyzed using gas chromatograph (9790II, Fuli, TCD) and calculated on the basis of O_2 peak area.

3. Results and discussion

3.1 Characterization of photocatalyst

Fig. 1 shows the typical X-ray diffractometry (XRD) patterns of as-prepared pure $BiVO_4$ and 2D/3D Bi_2O_3/$BiVO_4$@GO heterostructures. As can be seen, all the products have monoclinic $BiVO_4$. The intensive (221) peak (inset of **Fig. 1**) shows that the Bi_2O_3/$BiVO_4$@GO heterostructures have Bi_2O_3 phase, indicating coexistence

of Bi_2O_3 and $BiVO_4$ in the heterostructure photocatalysts. According to the results of whole pattern fitting and Rietveld refinement, the molar ratio of Bi_2O_3 and $BiVO_4$ is 4:96. In the synthesis step, GO solution enables the phase conversion and causes another product Bi_2O_3. It is worth noting that the modification of GO has no obvious influence on the XRD peaks of $Bi_2O_3/BiVO_4$, indicating that the vdW interaction between GO and $Bi_2O_3/BiVO_4$ does not alter the crystal structure of samples.

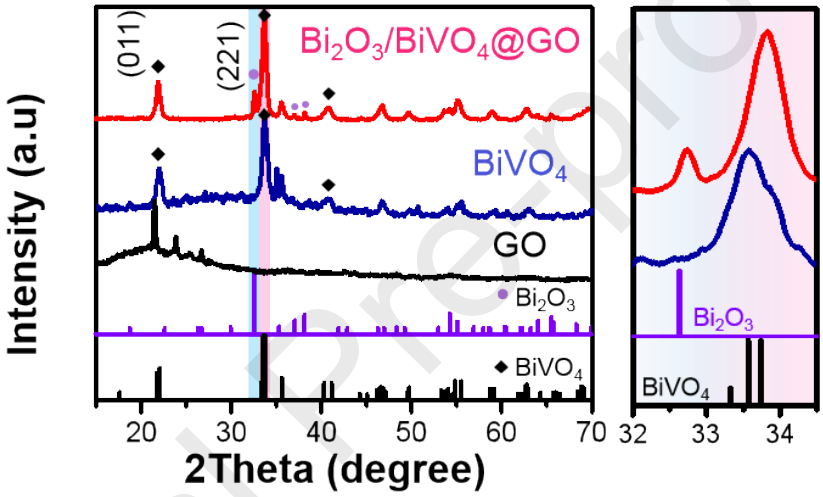

Fig. 1. XRD patterns of GO, $BiVO_4$ and $Bi_2O_3/BiVO_4$@GO.

The microstructure and morphology of 2D/3D $Bi_2O_3/BiVO_4$@GO vdW heterostructures synthesized by one-pot process described above were investigated by using SEM and TEM observations. **Fig. 2a-c** are typical SEM images of the products, which clearly reveals that the 2D/3D structure and the close integration between these three materials. As can be seen, mulberry-shape $Bi_2O_3/BiVO_4$ nanospheres have 500~600 nm and surrounded by GO layers to form heterostructures. Here, the GO layers act as the skeleton to enable the formation

of 2D/3D Bi_2O_3/$BiVO_4$@GO heterostructures. In the nucleation stage during the hydrothermal process, a large number of nuclei form rapidly and oriented by the van der Waals interactions on GO to establish vdW heterojunctions of Bi_2O_3/$BiVO_4$@GO, as schematically illustrated in **Fig. 2d**.

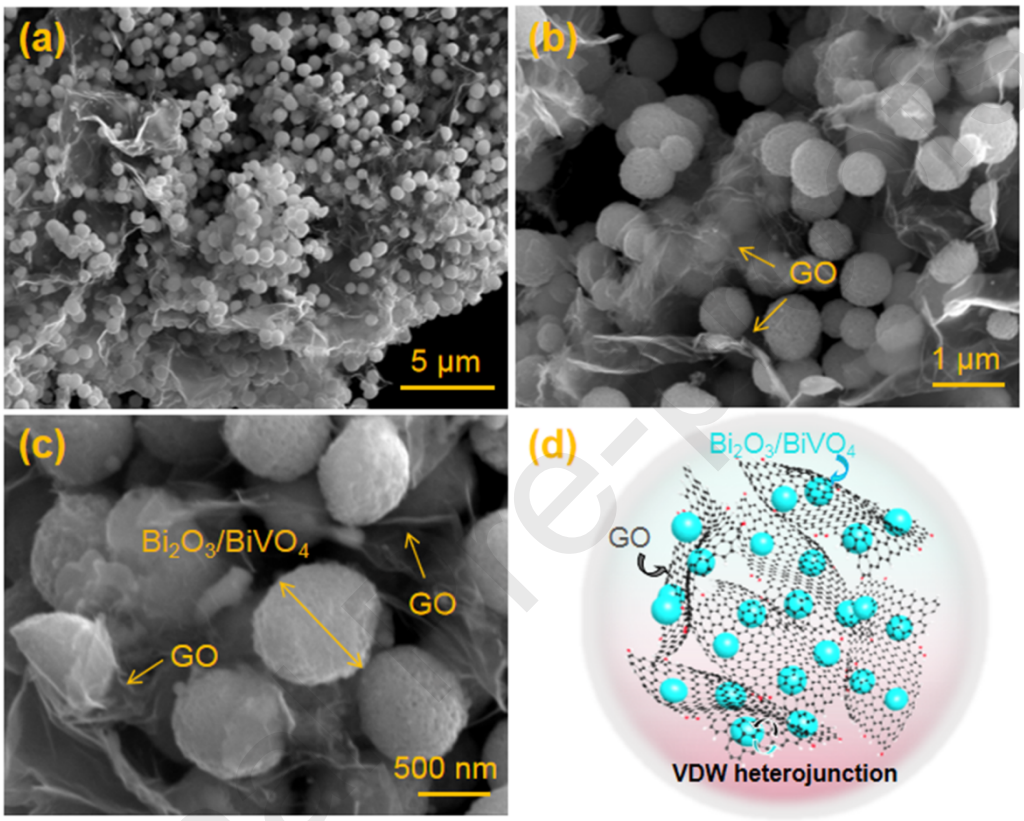

Fig. 2. (a-c) SEM images and (d) schematic illustration of Bi_2O_3/$BiVO_4$@GO.

Fig. 3a is a typical low-magnification TEM images of Bi_2O_3/$BiVO_4$@GO vdW heterostructures and shows that the 2D GO layers surround Bi_2O_3/$BiVO_4$ nanospheres by a self-assembly method. **Fig. 3b** is its corresponding high-resolution TEM (HRTEM) image, in which the crystal lattice distances of 0.47 nm and 0.31 nm can be measured, corresponding to the (011) plane of $BiVO_4$ and (221) plane of Bi_2O_3. This information

confirms the coexistence of $BiVO_4$ and Bi_2O_3. Fig. 3c are typical EDS elemental mappings of $Bi_2O_3/BiVO_4$ nanosphere, indicating that C, Bi, V, and O are co-existed in $Bi_2O_3/BiVO_4$ nanospheres.

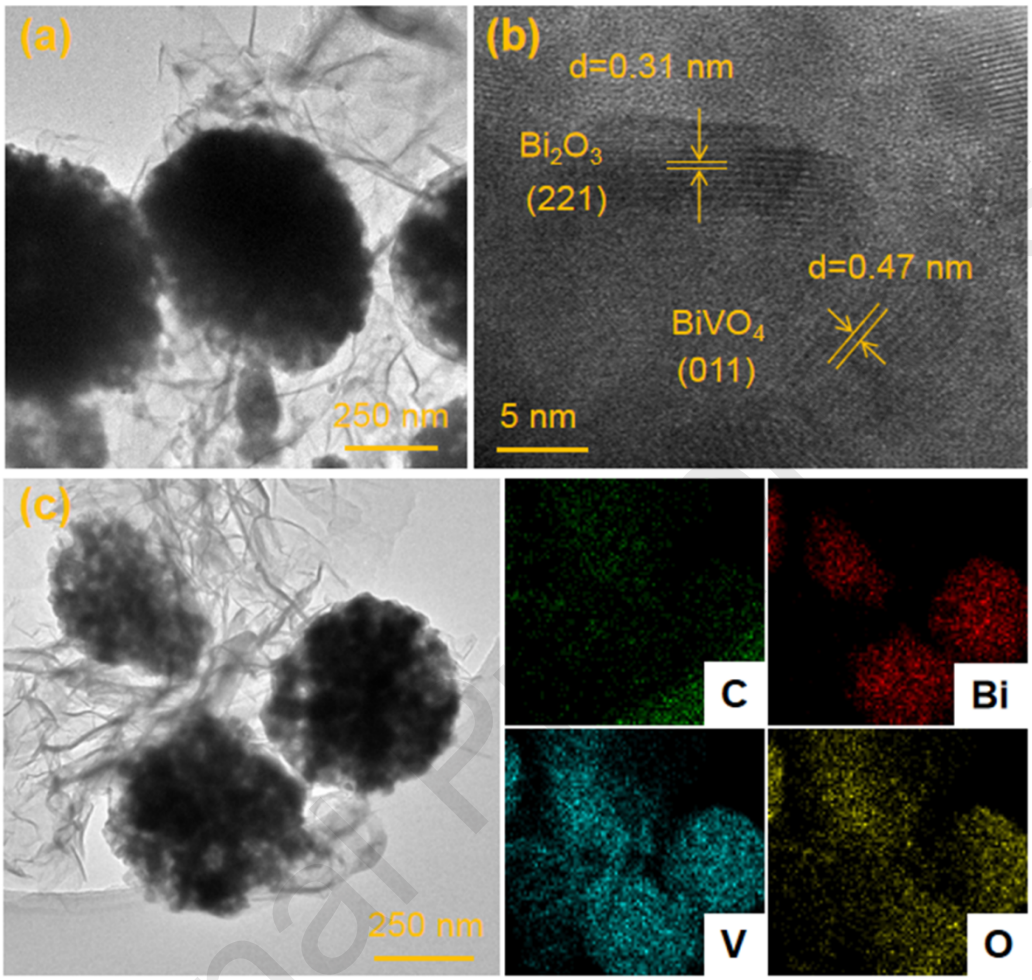

Fig. 3. (a) TEM image and (b) HRTEM image of $Bi_2O_3/BiVO_4$@GO. (c) EDS elemental mapping images of $Bi_2O_3/BiVO_4$@GO.

Raman spectroscopy was employed to investigate the bonding and structure of as-prepared pure $BiVO_4$ and 2D/3D $Bi_2O_3/BiVO_4$@GO heterostructures and the results are shown in **Fig. 4a**. The Raman peak at 817 cm^{-1} is due to the asymmetric and symmetric V-O stretching modes [27], confirming the presence of as-grown $BiVO_4$. In

addition, compared with pure $BiVO_4$, the spectrum of the $Bi_2O_3/BiVO_4$@GO displays D and G bands of the GO positioned at 1352 and 1589 cm^{-1} [28], which confirms that layered GO acts as the skeleton of 2D/3D structure. It can be noted that the intensity ratio of A to B in both $BiVO_4$ (0.13) and $Bi_2O_3/BiVO_4$@GO (0.1) was almost the same, demonstrating that the GO coating have not adversely affected the structure of $BiVO_4$.

The separation efficiency and recombination processes of charge carrier can be revealed by photoluminescence (PL) spectroscopy and the results are shown in **Fig. 4b**. During the charge recombination process, lower intensity in PL spectra refers to less photogenerated electron-hole pairs recombining, which can accelerate the photocatalytic reaction. It is worth noting that with GO layer coating, the PL peak intensity of 2D/3D $Bi_2O_3/BiVO_4$@GO heterostructure greatly decreases than that of $BiVO_4$, implying the lower charge recombination for $Bi_2O_3/BiVO_4$@GO heterostructure. This should be attributed to the conjugate structure and excellent carrier mobility of GO which can promote electron and mass transfer and suppress charge carrier recombination [6]. On the other hand, the fabrication of multi-dimensional 2D/3D vdW heterostructures not only enhances the interface contact but also reduces the photogenerated charges transfer distance to improve the separation of charge carriers [23].

To investigate the optical properties of as-prepared pure $BiVO_4$ and $Bi_2O_3/BiVO_4$@GO heterostructures, UV-vis absorption spectra were analyzed and the results are depicted in **Fig. 4c**. As can be seen, $BiVO_4$ and $Bi_2O_3/BiVO_4$@GO heterostructures exhibit evident absorption curves and show different absorption edges at around 450 nm and 530 nm, respectively. In comparison with pure $BiVO_4$, the absorption edge of

$Bi_2O_3/BiVO_4$@GO heterostructures has a distinct red shift, indicating the increased light absorption and enhanced photocatalytic activity. Besides, $Bi_2O_3/BiVO_4$@GO heterostructures have the significantly enhanced light absorption in the visible and even near-infrared (NIR) region, which can be attributed to the reduced energy gap and the formation of 2D/3D $Bi_2O_3/BiVO_4$@GO heterojunction. Based on above absorption spectra, the band gap (E_g) of samples can be calculated [29] and displayed in **Fig. 4d**. The estimated E_g values for $BiVO_4$ and $Bi_2O_3/BiVO_4$@GO are about 2.45 eV and 2.27 eV, indicating 2D/3D $Bi_2O_3/BiVO_4$@GO here structures have narrow optical E_g.

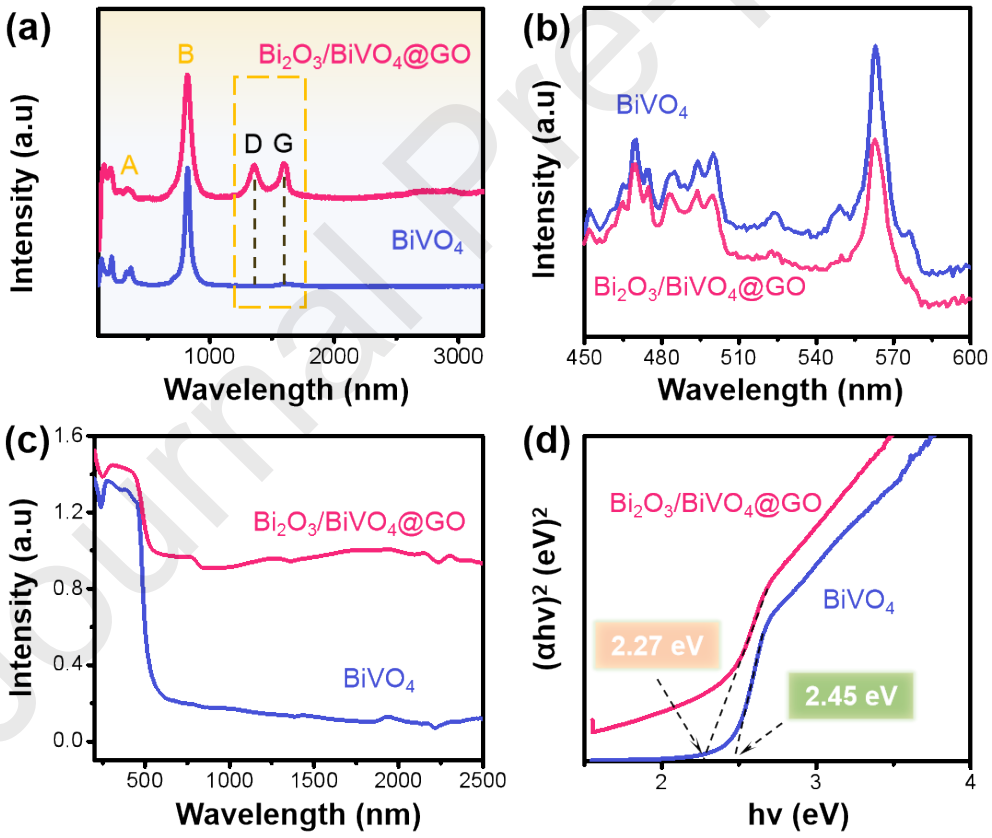

Fig. 4. (a) Raman spectra, (b) PL spectra, (c) UV-Vis absorption spectra and (d) bandgap of $BiVO_4$ and $Bi_2O_3/BiVO_4$@GO.

X-ray photoelectron spectroscopy (XPS) was further used to evaluate the surface chemical states of 2D/3D Bi_2O_3/$BiVO_4$@GO heterostructures and the results are shown in **Fig. 5**. In the high-resolution C 1s spectrum of GO (**Fig. 5a**), three major peaks located at 284.6, 285.6, and 288.26 eV were attributed to the binding energy of the sp^2 C=C bonds, sp^3 C-C bonds and O-C=O bonds, respectively. Two weak peaks at 158.52 eV and 163.74 eV are observed in Bi 4f spectrum (**Fig. 5b**), which correspond to the Bi $4f_{5/2}$ and Bi $4f_{7/2}$ binding energies of $BiVO_4$. Meanwhile, the two peaks at 159.29 eV and 164.36 eV are indexed to Bi $4f_{5/2}$ and Bi $4f_{7/2}$ in Bi_2O_3 (**Fig. 5b**), indicating that Bi element is presented as Bi^{3+} state, which suggests Bi_2O_3 exits in the heterostructures. As for the O 1s spectrum of **Fig. 5c**, the spectrum can be resolved into three characteristic peaks. The peak appearing at 529 eV can owe to the O^{2-} in $BiVO_4$, whereas the main peak at 530.4 eV was associated with C-O bonds in the GO. The other peak at 533.41 eV in O 1s spectrum is attributed to the Bi-O bonds in Bi_2O_3. The V 2p peak splits into two strong peaks at around 516.7 and 523.25 eV, which can be attributed to V $2p_{3/2}$ and V $2p_{1/2}$ binding energies of $BiVO_4$ (**Fig. 5d**).

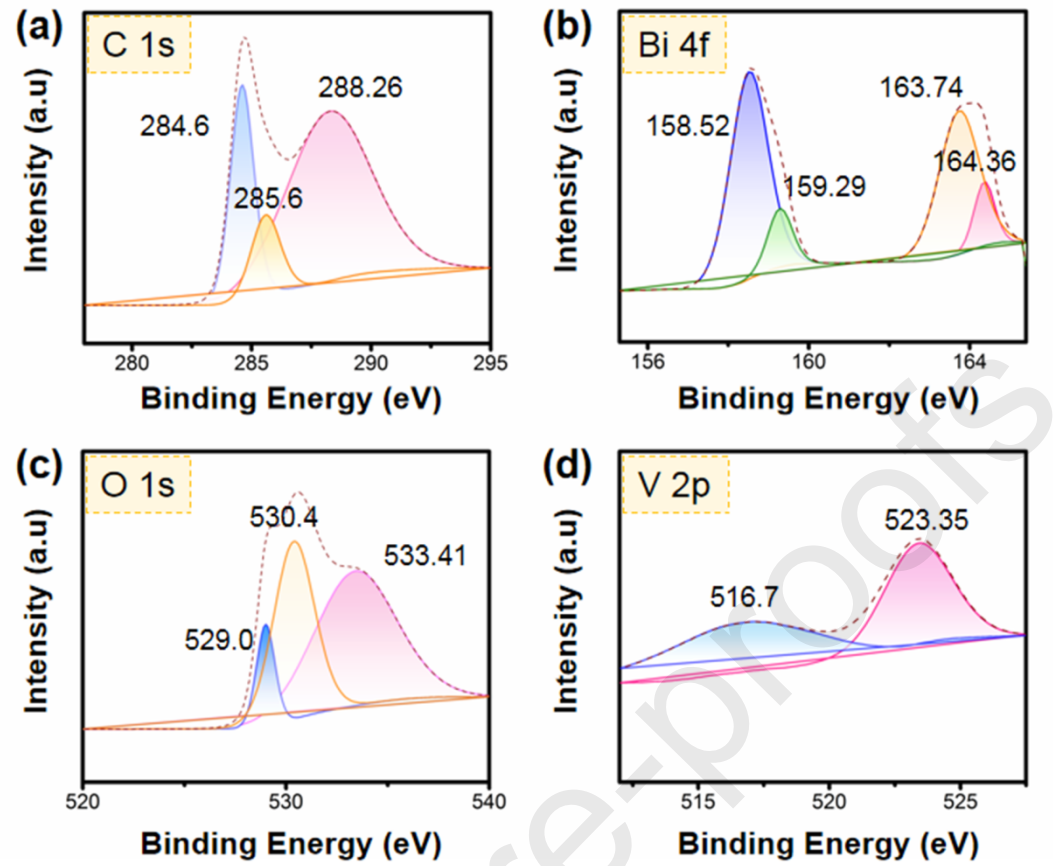

Fig. 5. XPS spectra of (a) C 1s, (b) Bi 4f, (c) O 1s and (d) V 2p for $Bi_2O_3/BiVO_4$@GO.

The typical functional groups of $BiVO_4$ and $Bi_2O_3/BiVO_4$@GO were investigated by Fourier transform infrared (FTIR) spectra, as shown in **Fig. 6a**. The spectra exhibit band at ~1726 cm^{-1} related to the C=O stretching of COOH groups at the edges of GO sheets. The bands at ~3500 cm^{-1} and 1630 cm^{-1} are related to OH stretching and bending vibrations [30-32]. The vibrational band at ~1400 cm^{-1} is attributed to the OH vibrations of H_2O molecules adsorbed on the sample surface. Furthermore, the band at ~739 cm^{-1} ascribes to the asymmetric stretching vibration of the ν_3 (VO_4) [33]. The band at ~526 cm^{-1} is ascribed to the Bi-O stretching pattern of Bi_2O_3 [34, 35], indicating the existence of Bi_2O_3 in the 2D/3D heterostructure. Additionally, it is obvious that the

primary bands of $BiVO_4$ and Bi_2O_3 are included in 2D/3D structure, implying that the Bi_2O_3/$BiVO_4$@GO heterostructures are fabricated successfully. Meanwhile, the spectra of 2D/3D Bi_2O_3/$BiVO_4$@GO heterostructure are similar to those of the main peaks of pure $BiVO_4$, demonstrating that the structure of $BiVO_4$ remains unchanged wrapped with the GO framework.

In order to further analyze the separation and transfer of photogenerated carriers in 2D/3D Bi_2O_3/$BiVO_4$@GO heterostructures, their reaction process was evaluated by photocurrents and electrochemical impedance spectroscopy (EIS). **Fig. 6b** displays the photocurrent responses of $BiVO_4$ and 2D/3D Bi_2O_3/$BiVO_4$@GO heterostructures. As can be seen, 2D/3D Bi_2O_3/$BiVO_4$@GO heterostructures show a much higher photocurrent density at a given potential comparing with that of pure $BiVO_4$, suggesting 2D/3D Bi_2O_3/$BiVO_4$@GO heterostructures have much higher transfer and separation efficiency of charge carriers. Moreover, the photocurrent remains stable after six repeated on/off light cycles, as suggested i**n Fig. 6b**. As shown in **Fig. 6c**, the comparison of the Nyquist plots exhibits a much smaller arc radius of 2D/3D Bi_2O_3/$BiVO_4$@GO heterostructures than that of pure $BiVO_4$, confirming smaller charge transfer resistance of 2D/3D Bi_2O_3/$BiVO_4$@GO heterostructures. Note that the GO loading in the heterostructure constitutes a framework for enhancing the transport of charge carriers while the 2D/3D structure serves to provide active pathway and massive reactive sites, providing a pathway for charge carrier migration rate.

Fig. 6d plots the photocatalytic O_2 evolution results for pure $BiVO_4$ and Bi_2O_3/$BiVO_4$@GO heterostructures were investigated within 5 h irradiation. Apparently, the pure $BiVO_4$ can catalyze the oxidation of water to O_2 and

the amount of evolved O_2 is 62.58 μmol. In contrast, $Bi_2O_3/BiVO_4$@GO heterostructures exhibits higher activity for O_2 evolution than pure $BiVO_4$ and gives 168.23 μmol of O_2, implying the superiority of 2D/3D heterostructures. As shown in **Fig. 6e**, the O_2 evolution rate of $Bi_2O_3/BiVO_4$@GO composite is 1828 μmol h^{-1} g^{-1}, nearly 3 times higher than that of the pure $BiVO_4$. **Fig. 6f** plots the compassion between our heterostructures and the reported [36-40]. As can be seen, our heterostructures show one of best performance for photocatalytic O_2 evolution activity. This remarkable increase in the O_2 evolution of $Bi_2O_3/BiVO_4$@GO is largely due to the structural coupling of the 2D GO and 3D $Bi_2O_3/BiVO_4$ heterojunction, allowing short electron transport distance and rapid charge transfer at the interface. Meanwhile, the heterojunction provides massive reactive sites and accelerates charge separation and transfer processes, taking advantage of the high specific surface area and good carrier mobility of GO framework. As shown in **Fig. 6g**, no obvious O_2 evolution rate decrease was observed after three cycles, demonstrating the stability of $Bi_2O_3/BiVO_4$@GO.

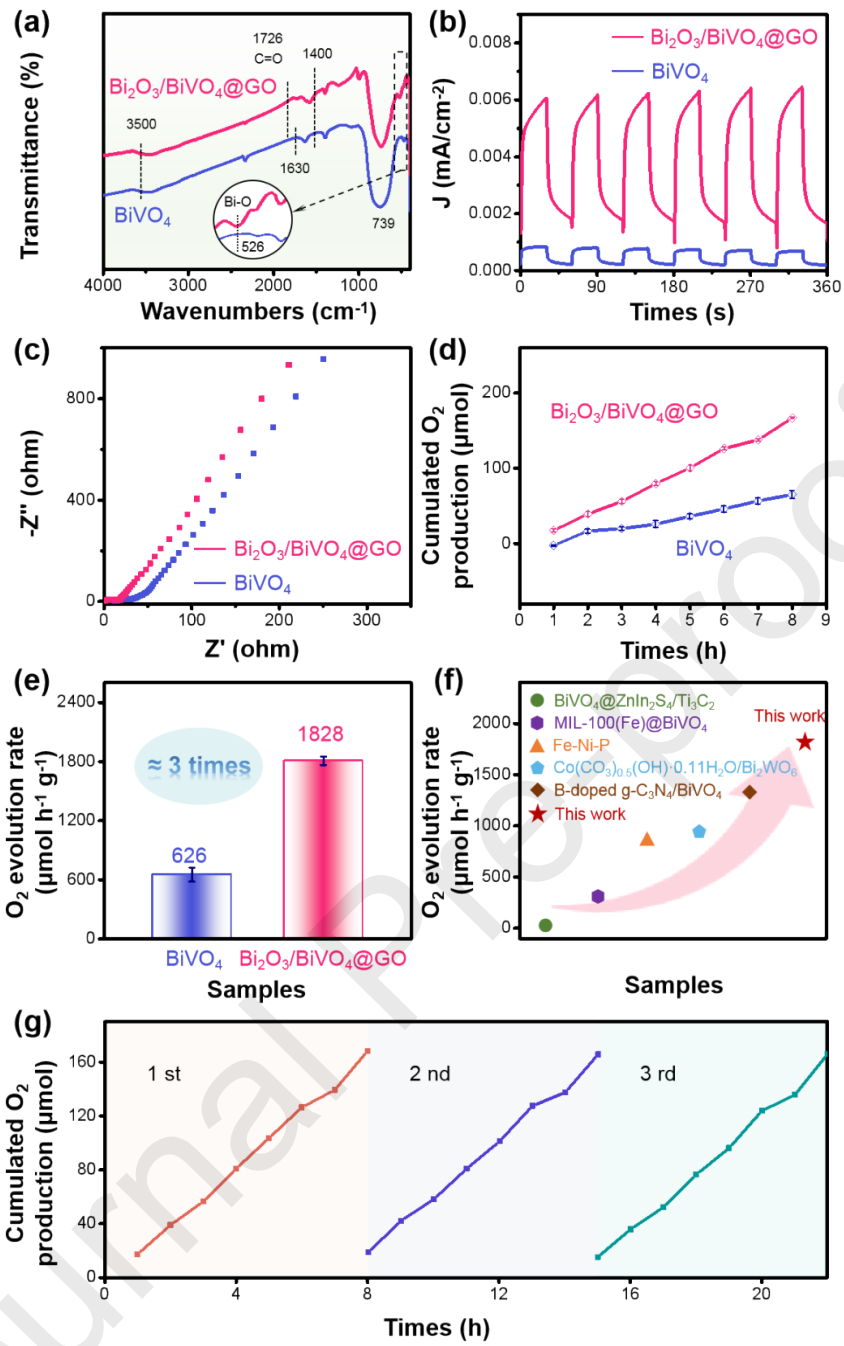

Fig. 6. (a) FTIR spectra of $BiVO_4$ and $Bi_2O_3/BiVO_4$@GO. (b) Photocurrent responses and (c) EIS Nyquist plot of $BiVO_4$ and $Bi_2O_3/BiVO_4$@GO. (d) Photocatalytic O_2 evolution performance and (e) O_2 evolution rates of $BiVO_4$ and $Bi_2O_3/BiVO_4$@GO. (f) Photocatalytic O_2 evolution rates of different samples. (g) Cyclic runs for the photocatalytic O_2 evolution over $Bi_2O_3/BiVO_4$@GO.

According to the above analysis and previous reports [23, 41], **Fig. 7** schematically illustrates the possible photocatalytic mechanism for the enhanced O_2 evolution activity of $Bi_2O_3/BiVO_4$@GO. The valence band of $BiVO_4$ is favorable for O_2 evolution [42]. Under the solar-simulated light irradiation, both $BiVO_4$ and Bi_2O_3 are excited and produce electron−hole pairs. The electrons on the valence band (VB) can be excited to the conduction band (CB) by the high energy photon, and the equal photogenerated holes (h^+) are generated. Generally, the photoinduced electrons (e^-) would migrate to the less negative CB, while the holes transfer to the less positive VB [43]. Therefore, due to the more positive CB and VB levels of Bi_2O_3, e^- will shift from $BiVO_4$ to Bi_2O_3 and h^+ migrates from Bi_2O_3 to $BiVO_4$, which can enhance charge separation and improve photocatalytic activity [44]. The h^+ transferred to $BiVO_4$ can easily oxidize H_2O to O_2. The interaction and proper energy band alignment between Bi_2O_3 and $BiVO_4$ is beneficial to promoting charge migration and suppressing photogenerated carrier recombination [45]. GO provides massive reactive sites and increases the interfacial contact with catalysts. In addition, the nanochannels provided by GO layers are beneficial to shortening migration distance and accelerating electrons transfer in the composite catalysts. GO plays the role of an electron transport mediator that accelerates the interfacial electron-transfer process from $BiVO_4$ to Bi_2O_3, strongly inhibiting the recombination of charge carriers and thus improving the photocatalytic activity. Moreover, GO leads to high specific surface area and provides massive reactive sites for h^+ oxidizing H_2O to O_2 [32, 46]. The improved photocatalytic performance is associated with the enhanced electronic conductivity caused by GO, and the synergetic effects between GO and $BiVO_4$ and Bi_2O_3 which reduce the recombination of photoinduced charge carriers. In this way, the

heterostructure of type-II is constructed and promotes the charge separation and transfer, in consistence with the results of PL, photocurrent and EIS, which is beneficial for enhanced O_2 evolution activity.

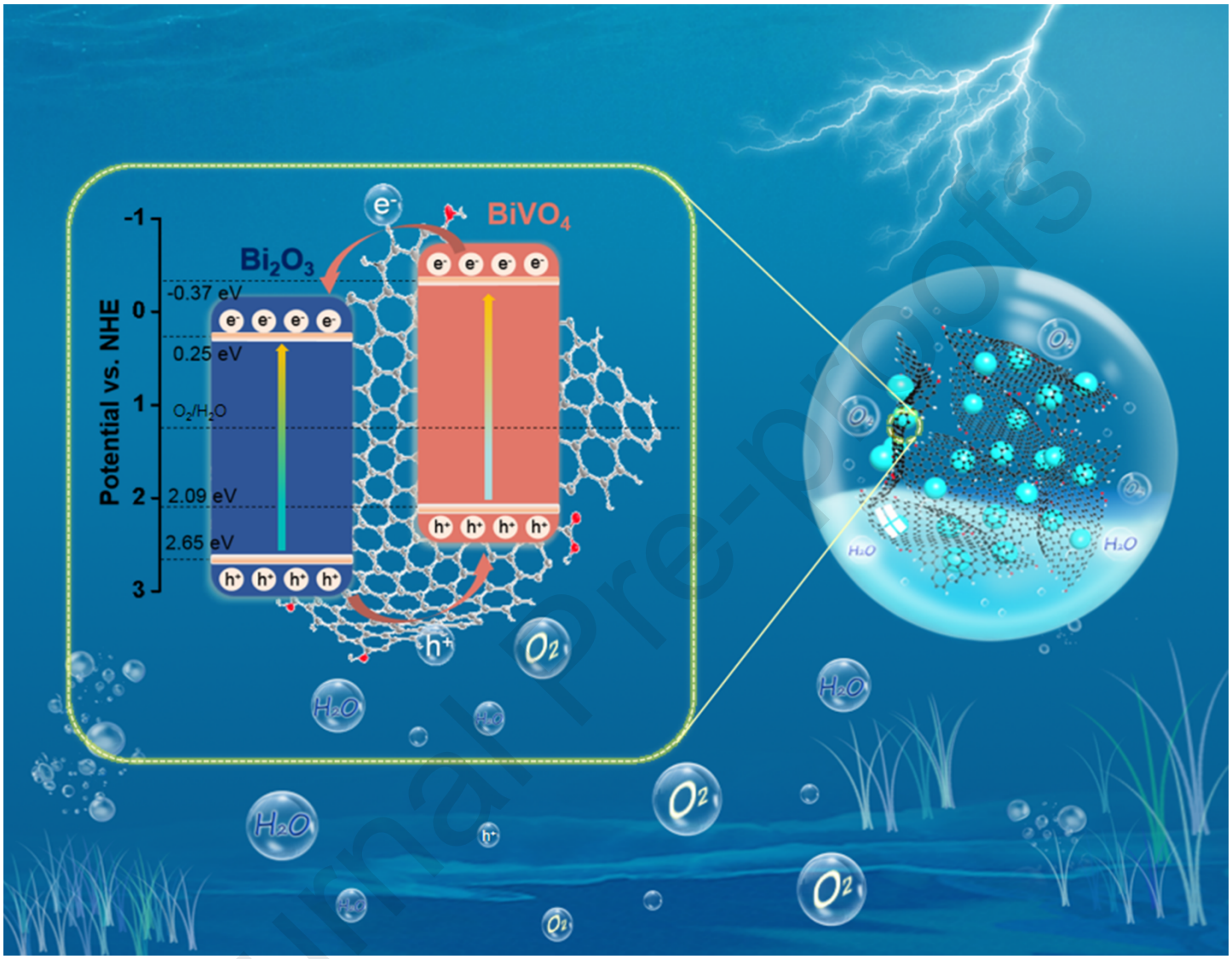

Fig. 7. The possible photocatalytic mechanism for the enhanced O_2 evolution activity of $Bi_2O_3/BiVO_4$@GO.

4. Conclusion

In conclusion, we use a facile self-assembly technique to fabricate 2D/3D $Bi_2O_3/BiVO_4$@GO vdW heterostructures, which exhibits an enhanced O_2 evolution rate of 1828 μmol h^{-1} g^{-1}, nearly 3 times than that of

pure $BiVO_4$. The enhanced photocatalytic activity may originate from the 2D/3D heterojunction with van der Waals interactions. The heterostructures composed of 2D GO and 3D $Bi_2O_3/BiVO_4$ is expected to play a significant role in promoting electron transfer and providing massive reactive sites. Hence, fabricating 2D/3D vdW heterostructures will create more possibilities in structural design of 2D materials and pave new channels to strengthen the connection between 2D and 3D materials.

Author contributions

Yaxin Bi: Investigation, Data curation, Writing - original draft. Yanling Yang: Conceptualization, Methodology, Writing - review & editing. Xiaolei Shi: Investigation, Writing - review & editing. Lei Feng: Investigation. Xiaojiang Hou: Investigation. Xiaohui Ye: Investigation. Li Zhang: Investigation. Guoquan Suo: Investigation. Jingeng Chen: Investigation. Zhi-Gang Chen: Conceptualization, Methodology, Visualization, Writing - review & editing.

Competing interests

The authors declare that they have no known competing financial interests or personal relationships that could have appeared to influence the work reported in this paper.

Acknowledgments

The authors acknowledge financial support from the National Natural Science Foundation of China (Grant Nos.: 51464020, 51101076, 51704188, 51802181, 61705125 and 51702199), Jiangxi Natural Science Foundation (Grant Nos.: 20161BAB206164 and 20161BBH80062), and Austrlian Research Council.

References

[1] Y. Li, R. Zhang, W. Zhou, X. Wu, H. Zhang, J. Zhang, Hierarchical MoS_2 hollow architectures with abundant Mo vacancies for efficient sodium storage, ACS Nano, 13 (2019) 5533-5540.

[2] R. Pathak, K. Chen, A. Gurung, K.M. Reza, B. Bahrami, F. Wu, A. Chaudhary, N. Ghimire, B. Zhou, W.-H. Zhang, Y. Zhou, Q. Qiao, Ultrathin bilayer of graphite/SiO_2 as solid interface for reviving Li metal anode, Adv. Energy Mater., 9 (2019) 1901486.

[3] H.R. Gutiérrez, N. Perea-López, A.L. Elías, A. Berkdemir, B. Wang, R. Lv, F. López-Urías, V.H. Crespi, H. Terrones, M. Terrones, Extraordinary room-temperature photoluminescence in triangular WS_2 monolayers, Nano Lett., 13 (2013) 3447-3454.

[4] C.-F. Fu, Q. Luo, X. Li, J. Yang, Two-dimensional van der Waals nanocomposites as Z-scheme type photocatalysts for hydrogen production from overall water splitting, J. Mater. Chem. A, 4 (2016) 18892-18898.

[5] C.-W. Chang, C. Hu, Graphene oxide-derived carbon-doped $SrTiO_3$ for highly efficient photocatalytic degradation of organic pollutants under visible light irradiation, Chem. Eng. J., 383 (2020) 123116.

[6] Y. Wang, K. Ding, R. Xu, D. Yu, W. Wang, P. Gao, B. Liu, Fabrication of $BiVO_4$/$BiPO_4$/GO composite photocatalytic material for the visible light-driven degradation, J. Clean Prod., 247 (2020) 119108.

[7] M. Liu, Y. Chen, J. Su, J. Shi, X. Wang, L. Guo, Photocatalytic hydrogen production using twinned nanocrystals and an unanchored NiSx co-catalyst, Nat. Energy, 1 (2016) 16151.

[8] J. Ran, W. Guo, H. Wang, B. Zhu, J. Yu, S.Z. Qiao, Metal-free 2D/2D phosphorene/g-C_3N_4 van der Waals heterojunction for highly enhanced visible-light photocatalytic H_2 production, Adv. Mater., 30 (2018) e1800128.

[9] A.K. Geim, I.V. Grigorieva, Van der Waals heterostructures, Nature, 499 (2013) 419-425.

[10] Q.L. He, H. Liu, M. He, Y.H. Lai, H. He, G. Wang, K.T. Law, R. Lortz, J. Wang, I.K. Sou, Two-dimensional superconductivity at the interface of a Bi_2Te_3/FeTe heterostructure, Nat Commun, 5 (2014) 4247.

[11] Y. Liu, J. Guo, E. Zhu, L. Liao, S.J. Lee, M. Ding, I. Shakir, V. Gambin, Y. Huang, X. Duan, Approaching the Schottky-Mott limit in van der Waals metal-semiconductor junctions, Nature, 557 (2018) 696-700.

[12] Z.R. Kudrynskyi, M.A. Bhuiyan, O. Makarovsky, J.D.G. Greener, E.E. Vdovin, Z.D. Kovalyuk, Y. Cao, A. Mishchenko, K.S. Novoselov, P.H. Beton, L. Eaves, A. Patanè, Giant quantum hall plateau in graphene coupled to an InSe van der Waals crystal, Phys. Rev. Lett., 119 (2017) 157701.

[13] S.A. Svatek, G.W. Mudd, Z.R. Kudrynskyi, O. Makarovsky, Z.D. Kovalyuk, C.J. Mellor, L. Eaves, P.H. Beton, A. Patanè, Graphene-InSe-graphene van der Waals heterostructures, J. Phys.: Conf. Ser., 647 (2015) 012001.

[14] P. Ajayan, P. Kim, K. Banerjee, Two-dimensional van der Waals materials, Phys. Today, 69 (2016) 38-44.

[15] S. Bawari, N.M. Kaley, S. Pal, T.V. Vineesh, S. Ghosh, J. Mondal, T.N. Narayanan, On the hydrogen evolution reaction activity of graphene–hBN van der Waals heterostructures, PCCP, 20 (2018) 15007-15014.

[16] R.K. Biroju, D. Das, R. Sharma, S. Pal, L.P.L. Mawlong, K. Bhorkar, P.K. Giri, A.K. Singh, T.N. Narayanan, Hydrogen Evolution Reaction Activity of Graphene–MoS_2 van der Waals Heterostructures, ACS Energy Lett., 2 (2017) 1355-1361.

[17] N.R. Finney, M. Yankowitz, L. Muraleetharan, K. Watanabe, T. Taniguchi, C.R. Dean, J. Hone, Tunable crystal symmetry in graphene–boron nitride heterostructures with coexisting moiré superlattices, Nat. Nanotechnol., 14 (2019) 1029-1034.

[18] H.-F. Wang, C. Tang, Q. Zhang, A review of graphene-based 3D van der Waals hybrids and their energy applications, Nano Today, 25 (2019) 27-37.

[19] B. Akram, B. Ni, X. Wang, Van der Waals integrated hybrid POM-Zirconia flexible belt-like superstructures, Adv. Mater., 32 (2020) 1906794.

[20] K.S. Novoselov, A. Mishchenko, A. Carvalho, A.H. Castro Neto, 2D materials and van der Waals heterostructures, Science, 353 (2016) aac9439.

[21] Y. Shi, W. Zhou, A.-Y. Lu, W. Fang, Y.-H. Lee, A. Hsu, S. Kim, K. Kim, H.Y. Yang, L. Li, J.-C. Idrobo, J. Kong, Van der Waals epitaxy of MoS_2 layers using graphene as growth templates, Nano Lett., 12 (2012) 2784-2791.

[22] D. Schwarz, Y. Noda, J. Klouda, K. Schwarzova-Peckova, J. Tarabek, J. Rybacek, J. Janousek, F. Simon, M.V. Opanasenko, J. Cejka, A. Acharjya, J. Schmidt, S. Selve, V. Reiter-Scherer, N. Severin, J.P. Rabe, P. Ecorchard, J. He, M. Polozij, P. Nachtigall, M.J. Bojdys, Twinned growth of metal-free, triazine-based photocatalyst films as mixed-dimensional (2D/3D) van der Waals heterostructures, Adv. Mater., 29 (2017) 1703399.

[23] R. Yang, Z. Zhu, C. Hu, S. Zhong, L. Zhang, B. Liu, W. Wang, One-step preparation (3D/2D/2D) $BiVO_4/FeVO_4$@rGO heterojunction composite photocatalyst for the removal of tetracycline and hexavalent chromium ions in water, Chem. Eng. J., 390 (2020) 124522.

[24] S. Shanavas, S. Mohana Roopan, A. Priyadharsan, D. Devipriya, S. Jayapandi, R. Acevedo, P.M. Anbarasan, Computationally guided synthesis of (2D/3D/2D) $rGO/Fe_2O_3/g\text{-}C_3N_4$ nanostructure with improved charge separation and transportation efficiency for degradation of pharmaceutical molecules, Appl. Catal. B-Environ., 255 (2019) 117758.

[25] Z. Zhang, H. Sun, X. Shao, D. Li, H. Yu, M. Han, Three‐dimensionally oriented aggregation of a few hundred nanoparticles into monocrystalline architectures, Adv. Mater., 17 (2005) 42-47.

[26] L. Zhang, R. Tong, S.E. Shirsath, Y. Yang, G. Dong, The crystalline/amorphous stacking structure of SnO_2 microspheres for the excellent NO photocatalytic performance, J. Mater. Chem. A, (2021) https://doi.org/10.1039/D1030TA12101K.

[27] A. Galembeck, O.L. Alves, $BiVO_4$ thin film preparation by metalorganic decomposition, Thin Solid Films, 365 (2000) 90-93.

[28] Y. Gao, D. Ma, C. Wang, J. Guan, X. Bao, Reduced graphene oxide as a catalyst for hydrogenation of nitrobenzene at room temperature, Chem. Commun., 47 (2011) 2432-2434.

[29] L. Wang, J. Liu, W. Song, H. Wang, Y. Li, J. Liu, Z. Zhao, J. Tan, Z. Duan, J. Deng, Experimental and DFT insights of $BiVO_4$ as an effective photocatalytic catalyst for N_2O decomposition, Chem. Eng. J., 366 (2019) 504-513.

[30] S.-Y. Chou, W.-H. Chung, L.-W. Chen, Y.-M. Dai, W.-Y. Lin, J.-H. Lin, C.-C. Chen, A series of BiOxIy/GO photocatalysts: synthesis, characterization, activity, and mechanism, RSC Adv., 6 (2016) 82743-82758.

[31] J. Ke, X. Duan, S. Luo, H. Zhang, H. Sun, J. Liu, M. Tade, S. Wang, UV-assisted construction of 3D hierarchical rGO/Bi_2MoO_6 composites for enhanced photocatalytic water oxidation, Chem. Eng. J., 313 (2017) 1447-1453.

[32] J.-P. Zou, J. Ma, Q. Huang, S.-L. Luo, J. Yu, X.-B. Luo, W.-L. Dai, J. Sun, G.-C. Guo, C.-T. Au, S.L. Suib, Graphene oxide as structure-directing and morphology-controlling agent for the syntheses of heterostructured graphene-Bi_2MoO_6/$Bi_{3.64}Mo_{0.36}O_{6.55}$ composites with high photocatalytic activity, Appl. Catal. B-Environ., 156-157 (2014) 447-455.

[33] R. Frost, D. Henry, M. Weier, W. Martens, Raman spectroscopy of three polymorphs of $BiVO_4$: Clinobisvanite, dreyerite and pucherite, with comparisons to $(VO_4)_3$-bearing minerals: namibite, pottsite and schumacherite, J. Raman Spectrosc., 37 (2006) 722-732.

[34] B. Shao, X. Liu, Z. Liu, G. Zeng, Q. Liang, C. Liang, Y. Cheng, W. Zhang, Y. Liu, S. Gong, A novel double Z-scheme photocatalyst Ag_3PO_4/Bi_2S_3/Bi_2O_3 with enhanced visible-light photocatalytic performance for antibiotic degradation, Chem. Eng. J., 368 (2019) 730-745.

[35] W. Luo, F. Li, Q. Li, X. Wang, W. Yang, L. Zhou, L. Mai, Heterostructured Bi_2S_3–Bi_2O_3 nanosheets with a built-in electric field for improved sodium storage, ACS Appl. Mater. Interfaces, 10 (2018) 7201-7207.

[36] P. Babu, S. Mohanty, B. Naik, K. Parida, Serendipitous assembly of mixed phase $BiVO_4$ on B-doped g-C_3N_4: an appropriate p–n heterojunction for photocatalytic O_2 evolution and Cr(VI) reduction, Inorg. Chem., 58 (2019) 12480-12491.

[37] X. Du, T. Zhao, Z. Xiu, Z. Xing, Z. Li, K. Pan, S. Yang, W. Zhou, $BiVO_4$@$ZnIn_2S_4$/Ti_3C_2 MXene quantum dots assembly all-solid-state direct Z-Scheme photocatalysts for efficient visible-light-driven overall water splitting, Appl Mater Today, 20 (2020) 100719.

[38] Q. Han, Y. Dong, C. Xu, Q. Hu, C. Dong, X. Liang, Y. Ding, Immobilization of metal–organic framework MIL-100(Fe) on the surface of $BiVO_4$: a new platform for enhanced visible-light-driven water oxidation, ACS Appl. Mater. Interfaces, 12 (2020) 10410-10419.

[39] B. He, H. Liu, Z. Lin, L. Yan, J. Ning, Y. Zhong, C. Zheng, Z. Zhang, Y. Hu, A new photocatalyst based on $Co(CO_3)_{0.5}(OH)\cdot 0.11H_2O/Bi_2WO_6$ nanocomposites for high-efficiency cocatalyst-free O_2 evolution, Chem. Eng. J., 359 (2019) 924-932.

[40] S. Li, J. Tan, Z. Jiang, J. Wang, Z. Li, MOF-derived bimetallic Fe-Ni-P nanotubes with tunable compositions for dye-sensitized photocatalytic H_2 and O_2 production, Chem. Eng. J., 384 (2020) 123354.

[41] Y. Lan, Z. Li, D. Li, W. Xie, G. Yan, S. Guo, Visible-light responsive Z-scheme Bi@β-Bi_2O_3/g-C_3N_4 heterojunction for efficient photocatalytic degradation of 2,3-dihydroxynaphthalene, Chem. Eng. J., 392 (2020) 123686.

[42] J.-B. Pan, B.-H. Wang, J.-B. Wang, H.-Z. Ding, W. Zhou, X. Liu, J.-R. Zhang, S. Shen, J.-K. Guo, L. Chen, C.-T. Au, L.-L. Jiang, S.-F. Yin, Activity and stability boosting of an oxygen-vacancy-rich $BiVO_4$ photoanode by NiFe-MOFs thin layer for water oxidation, Angew. Chem. Int. Ed., 59 (2020) 2-10.

[43] J.-B. Pan, S. Shen, W. Zhou, J. Tang, H.-Z. Ding, J.-B. Wang, L. Chen, C.-T. Au, S.-F. Yin, Recent progress in photocatalytic hydrogen evolution, Acta Phys. -Chim. Sin., 36 (2020) 1905068.

[44] J. Tang, B. Gao, J.-B. Pan, L. Chen, Z. Zhao, S. Shen, J.-K. Guo, C.-T. Au, S.-F. Yin, CdS nanorods anchored with CoS_2 nanoparticles for enhanced photocatalytic hydrogen production, Appl. Catal. A-Gen., 588 (2019) 117281.

[45] S. Lee, J. Song, Y.-R. Jo, K.S. Choi, J. Lee, S. Seo, T.L. Kim, H.W. Jang, C. Jeon, B.-J. Kim, B. Kim, S. Lee, In situ growth of nanostructured $BiVO_4$–Bi_2O_3 mixed-phase via nonequilibrium deposition involving metal exsolution for enhanced photoelectrochemical water splitting, ACS Appl. Mater. Interfaces, 11 (2019) 44069-44076.

[46] T.-D. Nguyen-Phan, V.H. Pham, E.W. Shin, H.-D. Pham, S. Kim, J.S. Chung, E.J. Kim, S.H. Hur, The role of graphene oxide content on the adsorption-enhanced photocatalysis of titanium dioxide/graphene oxide composites, Chem. Eng. J., 170 (2011) 226-232.

The captions of Figures and Tables

Fig. 1. XRD patterns of GO, $BiVO_4$ and $Bi_2O_3/BiVO_4$@GO.

Fig. 2. (a-c) SEM images and (d) schematic illustration of $Bi_2O_3/BiVO_4$@GO.

Fig. 3. (a) TEM image and (b) HRTEM image of $Bi_2O_3/BiVO_4$@GO. (c) EDS elemental mapping images of $Bi_2O_3/BiVO_4$@GO.

Fig. 4. (a) Raman spectra, (b) PL spectra, (c) UV-Vis absorption spectra and (d) bandgap of $BiVO_4$ and $Bi_2O_3/BiVO_4$@GO.

Fig. 5. XPS spectra of (a) C 1s, (b) Bi 4f, (c) O 1s and (d) V 2p for $Bi_2O_3/BiVO_4$@GO.

Fig. 6. (a) FTIR spectra of $BiVO_4$ and $Bi_2O_3/BiVO_4$@GO. (b) Photocurrent responses and (c) EIS Nyquist plot of $BiVO_4$ and $Bi_2O_3/BiVO_4$@GO. (d) Photocatalytic O_2 evolution performance and (e) O_2 evolution rates of $BiVO_4$ and $Bi_2O_3/BiVO_4$@GO. (f) Photocatalytic O_2 evolution rates of different samples. (g) Cyclic runs for the photocatalytic O_2 evolution over $Bi_2O_3/BiVO_4$@GO.

Fig. 7. The possible photocatalytic mechanism for the enhanced O_2 evolution activity of $Bi_2O_3/BiVO_4$@GO.

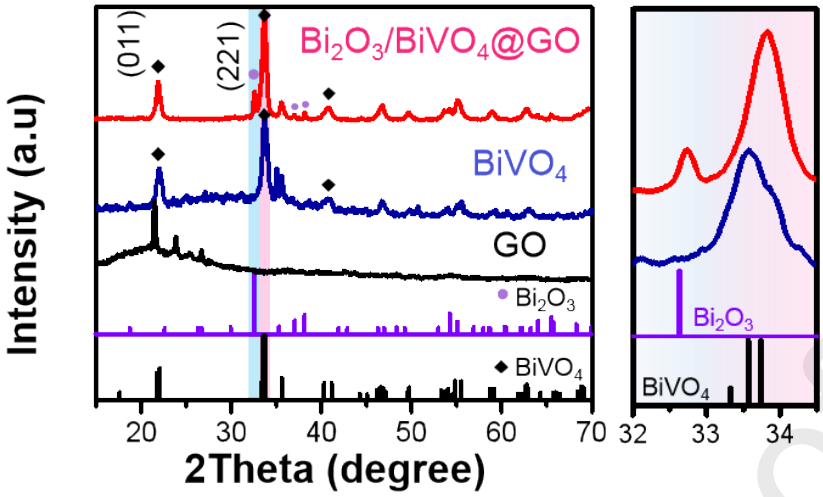

Fig. 1

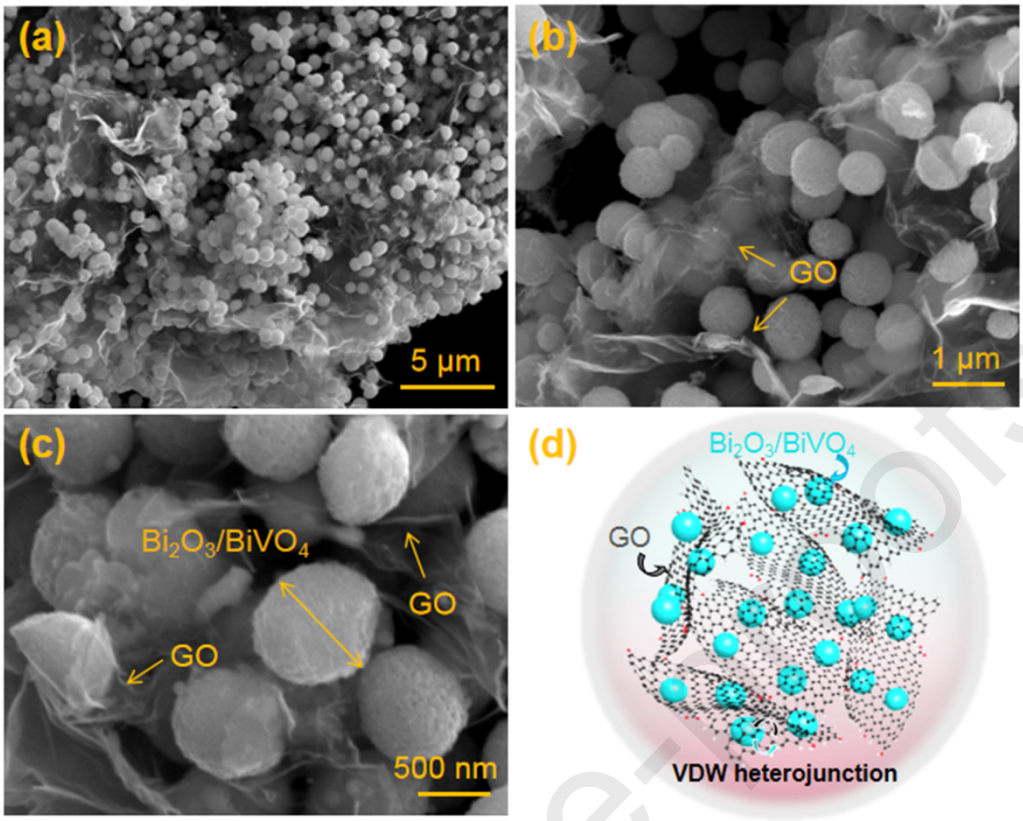

Fig. 2

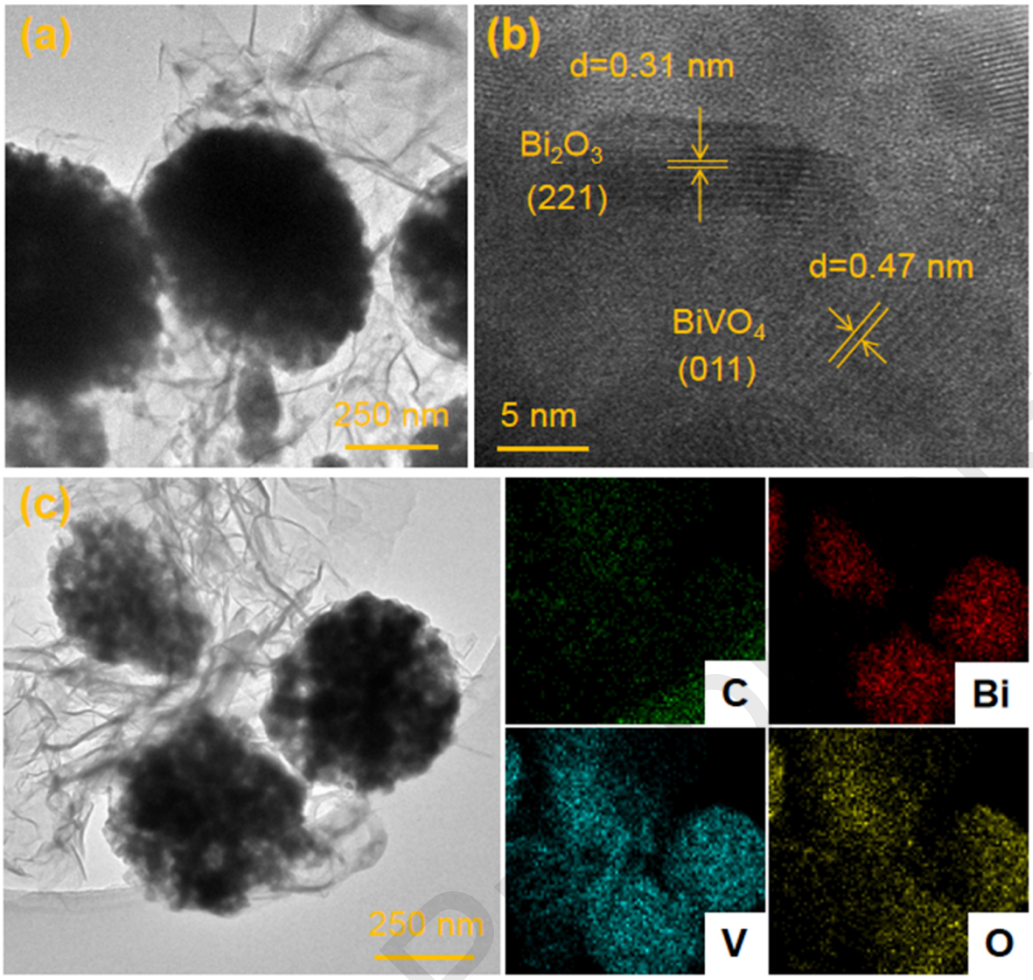

Fig. 3

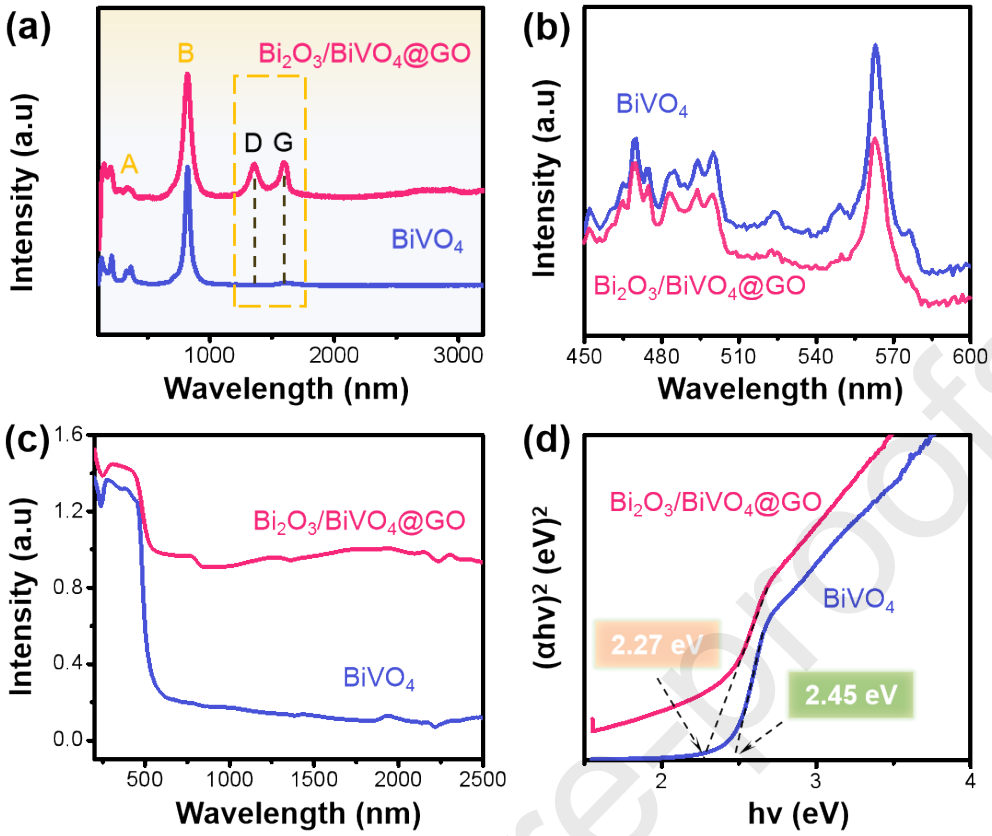

Fig. 4

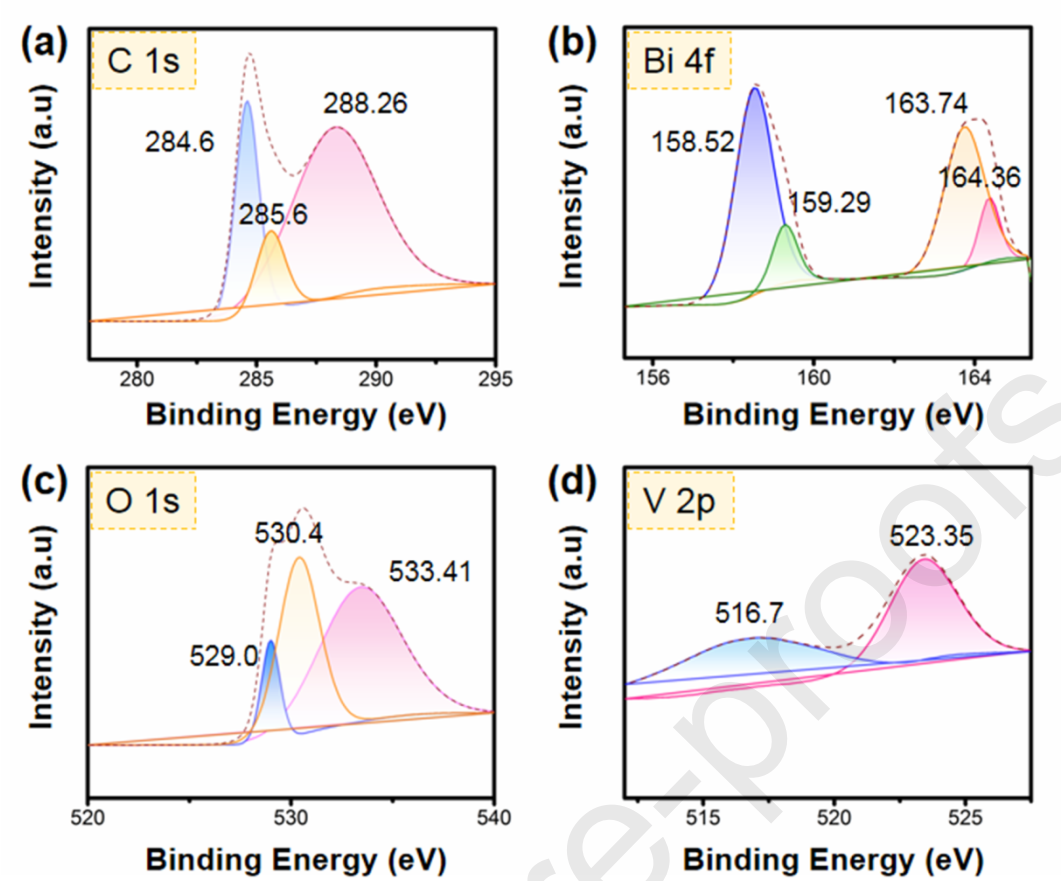

Fig. 5

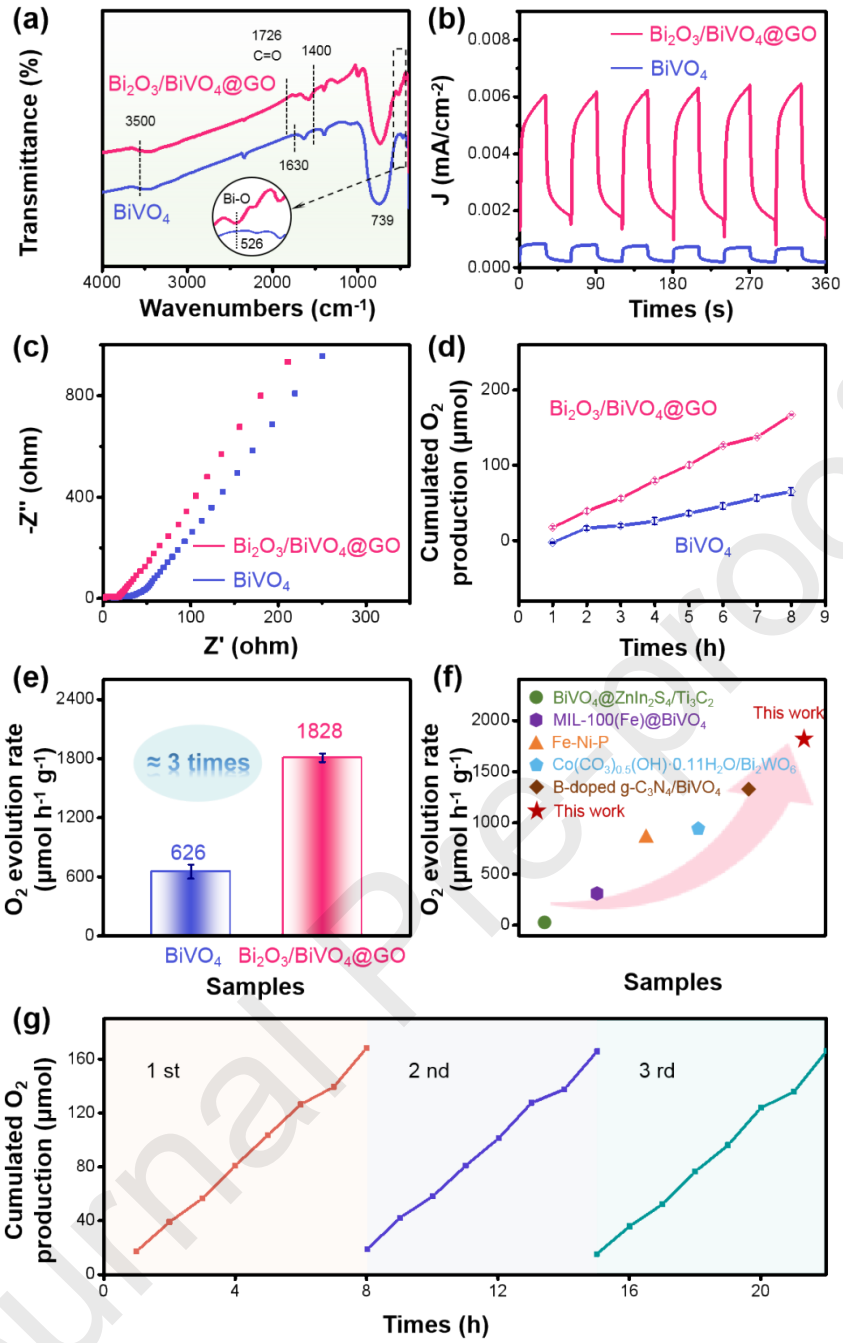

Fig. 6

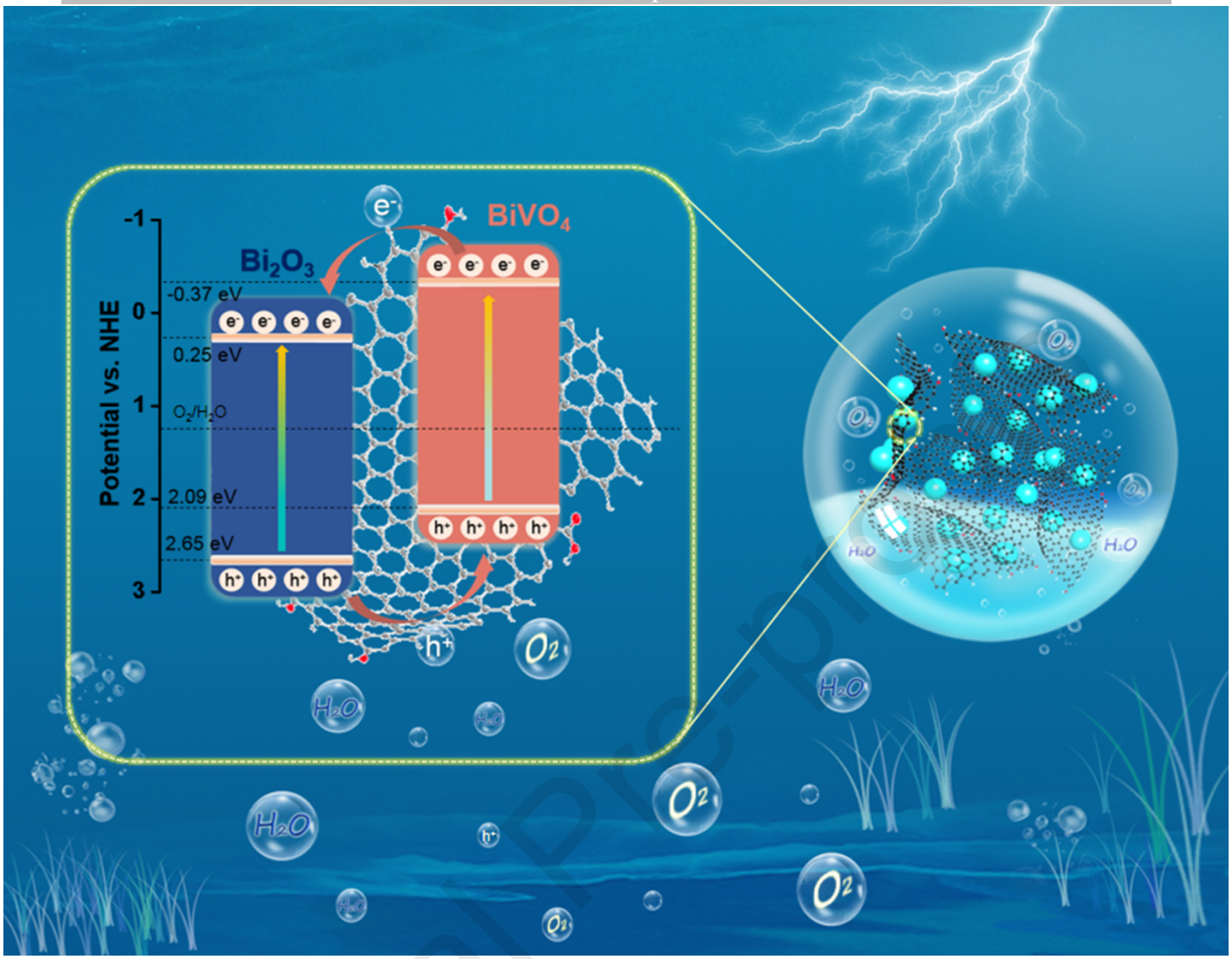
Potential vs. NHE
-1
0
1
2
3
Bi_2O_3
$BiVO_4$
-0.37 eV
0.25 eV
O_2/H_2O
2.09 eV
2.65 eV
e⁻
h⁺
O_2
H_2O

Fig. 7

TOC

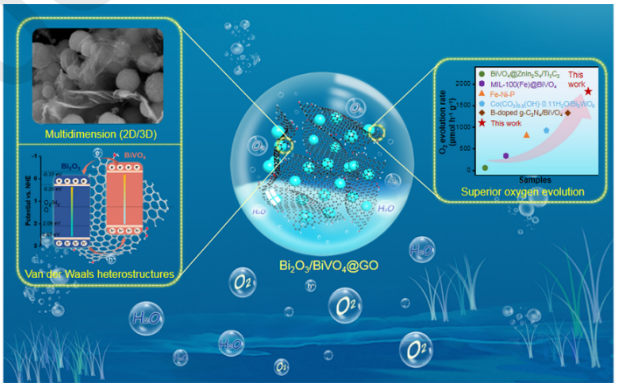
Multidimension (2D/3D)
Van der Waals heterostructures
$Bi_2O_3/BiVO_4$@GO
Superior oxygen evolution
Samples
This work

Highlight

- A multi-dimensional (2D/3D) $Bi_2O_3/BiVO_4$@GO is designed by self-assembly strategy;
- $Bi_2O_3/BiVO_4$@GO heterojunction is self-assembled by van der Waals interactions;
- The vdW heterostructure exhibits superior O_2 evolution of 1828 μmol h^{-1} g^{-1}.
- The strategy paves new avenue to fabricate multi-dimensional vdW heterostructures.

CRediT author statement

Yaxin Bi: Investigation, Data curation, Writing - original draft. **Yanling Yang**: Conceptualization, Methodology, Writing - review & editing. **Xiao-Lei Shi**: Investigation, Writing - review & editing. **Lei Feng**: Investigation. **Xiaojiang Hou**: Investigation. **Xiaohui Ye**: Investigation. **Li Zhang**: Investigation. **Guoquan Suo**: Investigation. **Jingeng Chen**: Investigation. **Zhi-Gang Chen**: Conceptualization, Methodology, Visualization, Writing - review & editing.

Declaration of interests

☒ The authors declare that they have no known competing financial interests or personal relationships that could have appeared to influence the work reported in this paper.

☐The authors declare the following financial interests/personal relationships which may be considered as potential competing interests: